DEXP: a fast method to determine the depth to the sources of potential fields

Article *in* Geophysics · January 2005

DOI: 10.1190/1.2144416

CITATIONS
68

READS
554

1 author:

Maurizio Fedi
University of Naples Federico II
265 PUBLICATIONS **3,286** CITATIONS

SEE PROFILE

GEOPHYSICS, VOL. 72, NO. 1 (JANUARY-FEBRUARY 2007); P. I1–I11, 15 FIGS., 1 TABLE.
10.1190/1.2399452

DEXP: A fast method to determine the depth and the structural index of potential fields sources

Maurizio Fedi[1]

ABSTRACT

We show that potential fields enjoy valuable properties when they are scaled by specific power laws of the altitude. We describe the theory for the gravity field, the magnetic field, and their derivatives of any order and propose a method, called here Depth from Extreme Points (DEXP), to interpret any potential field. The DEXP method allows estimates of source depths, density, and structural index from the extreme points of a 3D field scaled according to specific power laws of the altitude. Depths to sources are obtained from the position of the extreme points of the scaled field, and the excess mass (or dipole moment) is obtained from the scaled field values. Although the scaling laws are theoretically derived for sources such as poles, dipoles, lines of poles, and lines of dipoles, we give also criteria to estimate the correct scaling law directly from the data. The scaling exponent of such laws is shown to be related to the structural index involved in Euler Deconvolution theory. The method is fast and stable because it takes advantage of the regular behavior of potential field data versus the altitude z. As a result of stability, the DEXP method may be applied to anomalies with rather low SNRs. Also stable are DEXP applications to vertical and horizontal derivatives of a Newtonian potential of various orders in which we use theoretically determined scaling functions for each order of a derivative. This helps to reduce mutual interference effects and to obtain meaningful representations of the distribution of sources versus depth, with no prefiltering. The DEXP method does not require that magnetic anomalies to be reduced to the pole, and meaningful results are obtained by processing its analytical signal. Application to different cases of either synthetic or real data shows its applicability to any type of potential field investigation, including geological, petroleum, mining, archeological, and environmental studies.

INTRODUCTION

Several methods allow a semiautomated estimation of the source position and of a parameter characteristic of the source type, named structural index (e.g., Reid et al., 1990; Martelet et al., 2001). The structural index (SI) was developed in the frame of the Euler Deconvolution method and reflects the falloff rate of the potential field anomaly with distance. The SI can be important in the interpretation of potential field data because it characterizes the anomaly source in terms of simple shapes, thus helping to build a starting model for a forward method of interpretation. Euler deconvolution is defined for 1D and 2D data sets, and care must be taken to circumvent effects from noise and regional field interference. Our aim is to describe a new method to interpret potential field data on the basis of a meaningful, but until now unknown, property of 3D potential fields. The method, which we will call depth from extreme points (DEXP), applies to the Newtonian potential and to its nth-order derivatives and will be characterized by a high-degree of stability and accuracy in retrieving the location, the type (SI), and the excess source density.

The DEXP method is implemented in four stages:

1) Create a 3D data volume of the potential field. In practice, this means that data are needed both horizontally and vertically.
2) Scale the 3D field using specific laws — namely, the 3D field $f(\mathbf{r},\mathbf{r}_0)$, which originates from a source at $\mathbf{r}_0$, is transformed into a scaled field $W(\mathbf{r},\mathbf{r}_0)$.
3) Determine the depth to source, which involves a search for the extreme points of the scaled potential field. We will show that extreme points will occur for $W(\mathbf{r},\mathbf{r}_0)$ at points $\mathbf{r}(x,y,z)$ which are symmetrical (versus the xy-plane, Figure 1) to $\mathbf{r}_0(x_0,y_0,z_0)$, that is, at points enjoying the meaningful correspondence $x = x_0, y = y_0, z = -z_0$.
4) Compute the excess mass, or the excess dipole moment intensity for the magnetic field, from the value of the scaled potential field at the extreme points. The final result will then be a depth distribution of extreme points, excess mass values, and scaling exponents.

Manuscript received by the Editor December 23, 2005; revised manuscript received August 20, 2006; published online December 29, 2006.
[1]Università di Napoli Federico II, Dipartimento di Scienze della Terra, Largo san Marcellino 10, Napoli 80138, Italy. E-mail: fedi@unina.it.

THEORY OF THE DEXP TRANSFORMATION

In this paper, we consider any potential field, namely, the Newtonian potential and its derivatives of any degree n, comprising the gravity field, the magnetic field, and so on:

$$f(\mathbf{r}) = k\int_V \frac{\partial^n}{\partial z^n}\frac{M(\mathbf{r}_0)}{\|\mathbf{r}-\mathbf{r}_0\|_2}d^3\mathbf{r}_0, \tag{1}$$

where k is a physical constant related to the physical nature of the field, M stands for source density, and $\mathbf{r}$ and $\mathbf{r}_0$ are the position vectors at points P and Q in the harmonic and source regions, respectively (Figure 1). Here and throughout the paper, $\|.\|_2$ denotes the vector two-norm. We will consider either horizontal or vertical derivatives.

We first consider the gravity field f_1 ($n = 1$) from a single pole at some point $\mathbf{r}_0(x_0,y_0,z_0)$ with source density M. For simplicity, let us normalize it by the gravitational constant:

$$f_1(\mathbf{r}) = M\frac{(z-z_0)}{\|\mathbf{r}-\mathbf{r}_0\|_2^3} \tag{2}$$

and also assume M equal to 1. Then, let the source be at $\mathbf{r}_0(0,0,z_0)$ and consider the field at $x = x_0$, $y = y_0$, so to have

$$f_1(z) = \frac{1}{(z-z_0)^2}. \tag{3}$$

We define the scaling function τ as the derivative of the logarithm of a potential field f with respect to $\log(z)$:

$$\tau(z) = \frac{\partial\log[f(z)]}{\partial\log(z)}. \tag{4}$$

For τ_1,

$$\tau_1(z) = -\frac{2z}{z-z_0}. \tag{5}$$

This simple expression shows that τ_1, as expected, is singular in the source region at z_0. But in the harmonic region, for $z = -z_0$, $\tau_1 = -1$. This is shown in Figure 2 where the scaling function is drawn as a function of both the altitude z and the depth to source z_0. In fact, since

$$\tau_1(z=-z_0) = \left.\frac{\partial\log[f_1(z)]}{\partial\log(z)}\right|_{z=-z_0} = -1, \tag{6}$$

it follows that

$$\left.\frac{\partial\log[f_1(z)]}{\partial z}\right|_{z=-z_0} = -\left.\frac{\partial\log(z)}{\partial z}\right|_{z=-z_0}, \tag{7}$$

or

$$\left.\frac{\partial\{\log[f_1(z)]+\log(z)\}}{\partial z}\right|_{z=-z_0} = 0. \tag{8}$$

Hence, the function $\log f_1 + \log z$ has extreme points at $x = x_0$, $y = y_0$, $z = -z_0$. In Figure 3, we show the surface $\log(f_1) + \log(z)$ for $x = x_0$, $y = y_0$, while z and z_0 are free variables. As one may easily observe, for poles at any depth z_0, a curve occurs having an extreme point at $z = -z_0$. From equation 8, we may also argue that

$$\left.\frac{\partial z f_1}{\partial z}\right|_{z=-z_0} = 0. \tag{9}$$

This means that the function obtained by scaling the gravity field with a power law of the altitude z and exponent equal to 1

$$W_{g1} = f_1 z \tag{10}$$

will have meaningful extreme points at $x = x_0$, $y = y_0$, $z = -z_0$ (Figure 4). We call this function the DEXP transformation W_{g1} of the gravity field.

Owing to the above correspondence of $x = x_0$, $y = y_0$, $z = -z_0$, we may also express W_{g1} as a function of source coordinates $\mathbf{r}_0(x_0,y_0,z_0)$ instead of as a function of $\mathbf{r}$ $(x,y,z=-z_0)$. Because we assumed a positive density contrast for the source, the extreme points here considered for $f_1 z$ are all absolute maxima. It is easy to understand that, for a negative density contrast, the corresponding extreme point will be an absolute minimum.

These results are not restricted only to the gravity field. For example, we can compute W in the case of the vertical derivative of the

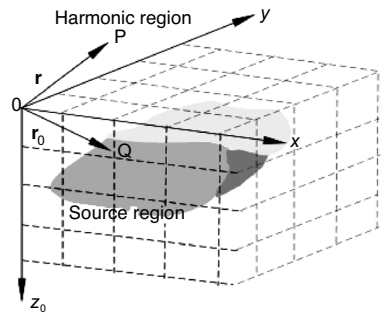

Figure 1. Position vectors for DEXP transformation theory. The position vectors $\mathbf{r}$ and $\mathbf{r}_0$ indicate field points P($\mathbf{r}$) in the harmonic region and source points Q($\mathbf{r}_0$) in the source region.

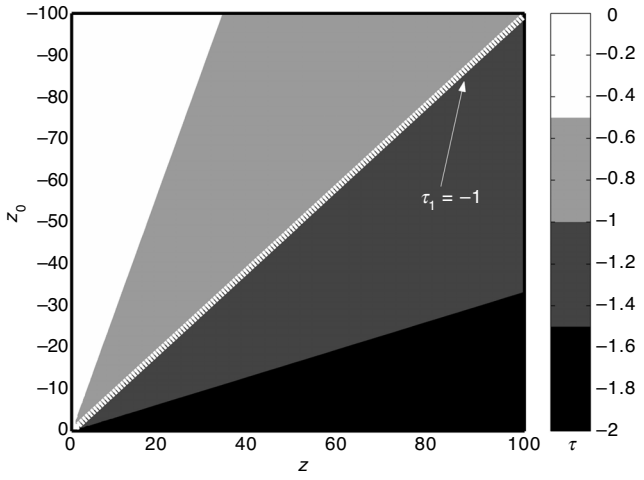

Figure 2. The scaling function τ_1 for $n = 1$ potential fields. The key of the DEXP transformation is that τ_1 is equal to -1 when $z = -z_0$ (equation 6). A similar behavior holds for higher orders of n according to the law: $\tau_n = -(n+1)/2$ when $z = -z_0$ (equation 16).

gravity field (i.e., for $n = 2$) or, equivalently, that of the magnetic field. In this case, assuming $M = 1$ and considering the source at $\mathbf{r}_0(0,0,z_0)$ and for $y = 0$, we have

$$f_2(x,z) = \frac{2(z - z_0)^2 - x^2}{[x^2 + (z - z_0)^2]^{5/2}}, \tag{11}$$

where the field is again normalized by k.

So, at $x = x_0 = 0$, we have

$$\tau_2(z) = \frac{\partial \log(f_2)}{\partial \log(z)} = -3\frac{z}{z - z_0}. \tag{12}$$

Hence,

$$\tau_2(z = -z_0) = \left.\frac{\partial \log[f_2(z)]}{\partial \log(z)}\right|_{z = -z_0} = -1.5, \tag{13}$$

so that we obtain the following scaling function $W_2(x,z)$:

$$W_2 = f_2 z^{3/2} = \frac{2(z - z_0)^2 - x^2}{[x^2 + (z - z_0)^2]^{5/2}} z^{3/2}. \tag{14}$$

By using this procedure, we can obtain a more general definition of the DEXP transformation that determines any nth vertical derivative of the Newtonian potential of a pole source, $f_n(z) = 1/(z - z_0)^{n+1}$.

We find for the scaling function τ_n:

$$\tau_n = \frac{\partial \log[f_n(z)]}{\partial \log(z)} = -\frac{(n + 1)z}{z - z_0}, \tag{15}$$

so that, at $z = -z_0$,

$$\tau_n(z = -z_0) = \left.\frac{\partial \log[f_n(z)]}{\partial \log(z)}\right|_{z=-z_0} = -\frac{(n + 1)}{2}. \tag{16}$$

Hence, meaningful extreme points occur at $x = x_0$, $y = y_0$, $z = -z_0$ for the scaled function

$$W_n = z^{\alpha_n} f_n, \tag{17}$$

where

$$\alpha_n = -\tau_n(z = -z_0) = 0.5(n + 1) \tag{18}$$

are the scaling exponents of the DEXP transformation of order n.

In the following text, depending on the potential field order and on the type of potential field, we, respectively, refer to the potential field as the scaled gravity field W_{g1}, the scaled magnetic field W_{m2}, the scaled Gravity Vertical Gradient W_{g2}, and so on.

Estimating the excess mass

One important aspect of the DEXP transformation is the possibility to estimate the mass excess M from the value of the scaled gravity field $W_{g1}(\bar{\mathbf{r}}_0)$, where $\bar{\mathbf{r}}_0$ indicates its extreme points. For a single pole, we find (see equation 10)

$$W_{g1}(\bar{\mathbf{r}}_0) = \left.\frac{\gamma M z}{(z - \bar{z}_0)^2}\right|_{z = -\bar{z}_0} = \frac{\gamma M}{4\bar{z}_0}, \tag{19}$$

where g is the gravitational constant, so that

$$M = \frac{4W_{g1}(\bar{\mathbf{r}}_0)\bar{z}_0}{\gamma}, \tag{20}$$

from which the density of a uniformly dense sphere of radius a is

$$\rho = \frac{4W_{g1}(\bar{\mathbf{r}}_0)\bar{z}_0}{4/3\,\pi\gamma a^3}. \tag{21}$$

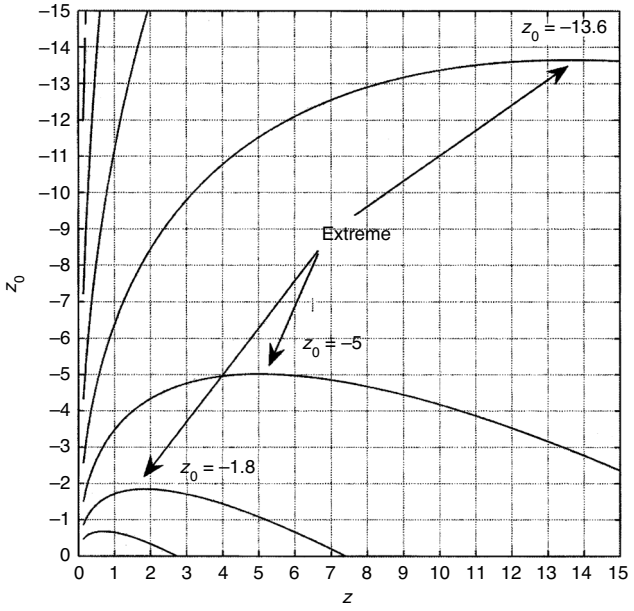

Figure 3. The function, $\log f_1 + \log z$, at $x = x_0$, $y = y_0$. Observing the surface, $\log[f_1(z,z_0)] + \log(z)$, we clearly see that, for poles at any depth z_0, a curve occurs having an extreme point at $z = -z_0$.

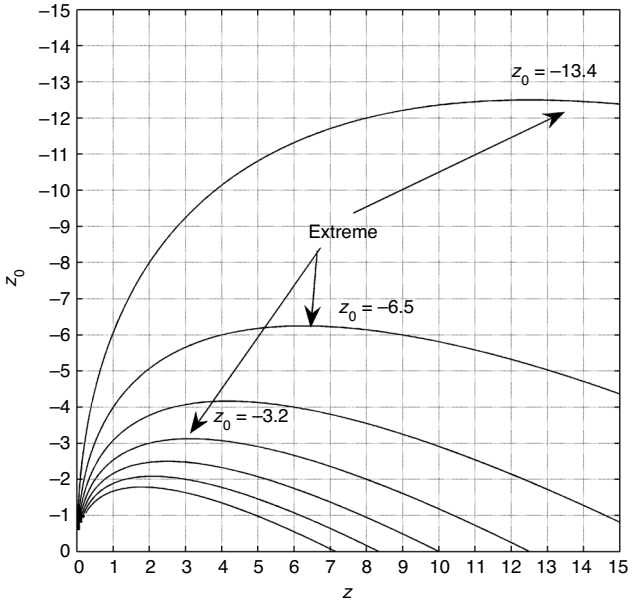

Figure 4. The function $f_1 z$ at $x = x_0$, $y = y_0$. Observing the surface $f_1(z,z_0)z$, we see that, for poles at any depth z_0, a curve occurs having an extreme point at $z = -z_0$.

Similar formulas may be obtained for any nth-order vertical derivative of the Newtonian potential, such as the first-order vertical derivative of the gravity field ($n = 2$):

$$M = \frac{4W_{g2}(\bar{\mathbf{r}}_0)\bar{z}_0^{3/2}}{\gamma}, \tag{22}$$

and the second-order vertical derivative of the gravity field ($n = 3$):

$$M = \frac{8W_{g3}(\bar{\mathbf{r}}_0)\bar{z}_0^{2}}{3\gamma}. \tag{23}$$

Similarly, for the magnetic field, the excess in the dipole moment intensity $|\mathbf{M}|$ may be estimated from W_{m2} using the formula

$$|\mathbf{M}| = 4W_{m2}(\bar{\mathbf{r}}_0)\bar{z}_0^{3/2}. \tag{24}$$

Obviously, we mean that sources contributing to the annihilator (Parker, 1977) are not included in the estimate of the dipole moment intensity because they are expressly defined as sources causing a zero-strength anomaly.

One-point sources

A general, or extended, source generates a field that cannot be explained by a simple pole source, unless the measurement plane is so distant that any term of order $p > 1$ becomes negligible in the multipole expansion of the field. In this case, the equations developed for a single pole (equations 17 and 18) will give a reasonable approximation to the problem. For instance, Kellogg (1967) gives the first two terms of the multipolar expansion of the gravity potential of a homogeneous cube of side d:

$$f_0(r) \approx \gamma\frac{M}{r} - \frac{7\gamma Md}{60r^9}[3r^4 - 5(x^4 + y^4 + z^4)], \tag{25}$$

thus showing that its effect, and also that of its derivatives, may be quite well approximated by the first pole term, provided that the distance-to-source is large enough.

Real sources may be defined as source distributions within finite volumes with arbitrary shapes. However, we may often approximate real source distributions in terms of semi-infinite solids and volumeless figures (points, lines, surfaces). This is especially true for equivalent representations of some real sources from their fields, such as those related to the infinite set of concentric spheres of equal mass, which are all equivalent to a point-mass at their center. Besides the sphere equivalence, we have also that of infinite cylinders (used for pipes, ridges, valleys, tunnels, volcanic necks) and that of sills, dikes, steps, or plates which are respectively equivalent or close to volume-less theoretical models such as lines or planes. From a geometrical point of view, these sources are commonly defined as one-point sources, meaning that we need the coordinates of just one singular point (the center, the edge, or the vertex point of the real figure) to define them. A thin dike or a finite step with large, but limited, depth extent will instead be better sketched by a two-point source characterized by two singular source points.

Similar to the theory of Euler deconvolution (e.g., Reid et al., 1990; Stavrev, 1997; Salem and Ravat, 2003; Cooper, 2004; Keating and Pilkington, 2004) or to that of the continuous wavelet transform (CWT) (e.g., Hornby et al., 1999; Sailhac and Gibert, 2003, Fedi et al., 2004), it is therefore useful to define the DEXP transformation properties of one-point sources. By the same approach used for computing the DEXP transformation of a pole source, we may outline the theory for any one-point source. For instance, we may study the infinite horizontal cylinder (e.g., Telford et al., 1990). Putting $M = 1$, $x_0 = y_0 = y = 0$, we have, for the gravity field,

$$f_1(x,z) = \frac{2(z - z_0)}{x^2 + (z - z_0)^2}, \tag{26}$$

where the field is again normalized by the gravitational constant. The scaling function τ_1 at $x = x_0 = 0$ is

$$\tau_1(z) = \frac{\partial \log(f_1)}{\partial \log(z)} = -\frac{z}{z - z_0}, \tag{27}$$

so that

$$\alpha_1 = 0.5 \tag{28}$$

and

$$W_1(x,z) = f_1(x,z)z^{1/2} = \frac{2(z - z_0)^2}{x^2 + (z - z_0)^2}z^{1/2}. \tag{29}$$

More generally, for the nth vertical derivative of the gravity potential of this kind of source, one may again use equation 17:

$$W_n(z) = z^{\alpha_n}f_n(z), \tag{30}$$

but the scaling exponents α_n of order n are now given by

$$\alpha_n = 0.5n. \tag{31}$$

Another kind of source is that of the semi-infinite horizontal thin sheet (e.g., Telford et al., 1990):

$$f_1(x,z) = 2\left[\frac{\pi}{2} - \text{a tan}\left(\frac{x - x_0}{z - z_0}\right)\right], \tag{32}$$

where we assumed $M = 1$ and normalized with respect to γ. We find for this source that $\alpha_1 = 0$, so that no DEXP transformation should, in principle, be applied to the field of this kind of source. But we can consider instead its horizontal derivative, which is a bell-shaped function:

$$f_2(x,z) = \frac{\partial f_1}{\partial x} = \frac{2(z - z_0)}{(z - z_0)^2 + (x - x_0)^2}. \tag{33}$$

In this case, we find $\alpha_2 = 0.5$, thus allowing us to use the DEXP transformation. The general rule for this kind of source is that we may apply the DEXP transformation only to derivatives of order $n \geq 2$ using

$$\alpha_n = 0.5(n - 1). \tag{34}$$

Table 1 describes the scaling exponents for typical one-point sources classified in four classes, from A to D. We also report the source parameter involved in the well-known theory of the Euler deconvolution (Reid et al., 1990, Stavrev, 1997, Mushayandebvu et al., 2001), called structural index (SI). Because the structural index increments by one with n, here we will use S_n, a slightly different notation, as a replacement for SI. For instance, S_1 will denote SI for gravity anomalies and S_2 will denote SI for magnetic anomalies. We note immediately that a clear relationship exists between α_n and S_n, which may be expressed as

$$S_n = 2\alpha_n. \tag{35}$$

This depends on the fact that both S_n and α_n are source parameters reflecting the type of source and the falloff rate of their fields. However, there are some differences: We saw that, in the gravity case, the DEXP transformation is not applicable to sources, such as a semi-infinite plane, because the scaling exponent is zero, thus meaning that the scaling would be ineffective. Otherwise, we may study this kind of source using a higher order of potential field, such as its gradient. For a contact type of source ($S_n = -1$), we indicate within brackets the scaling exponent ($\alpha_1 = -0.5$) because it may be derived from either

$$\alpha_n = 0.5(n - 2), \tag{36}$$

or from equation 35, this exponent being valid only for $n \geq 3$. To analyze its field, consistent results are determined using its derivatives of order $n \geq 3$, such as $\partial^2 f_1/\partial x \partial z$.

PERFORMING DEXP

Keeping in mind the scheme described in the Introduction and the theory described in the preceding sections, we show in this section how to apply the DEXP technique to the interpretation of potential field anomalies.

The first step is to form a 3D data set for the potential field under consideration. It is rare to have data sets available at different elevations, except for repeat surveys at both sea and airborne levels. We may, nevertheless, overcome this problem using the well-known formula of upward continuation:

$$G(x,y,z) = \frac{1}{2\pi} \int \int_S G(\xi,\eta,z_m) \times \frac{z - z_m}{[(x-\xi)^2 + (y-\eta)^2 + (z-z_m)^2]^{3/2}} d\xi d\eta, \tag{37}$$

which we obtain by using the Green's theorem (e.g., Baranov, 1975). In equation 37, $z > z_m$, and S is an infinitely extended region. This equation is a convolution integral and linearly relates the data at some level z_m to those at higher levels. In practice, we may only use an approximate discrete version of equation 37. Hence, some care must be taken that continuation of a finite and discrete set of potential field data, known over a finite region S, could yield upwardly continued data as accurately as possible. Note that this problem is the same as that which occurs in defining the CWT using a Poisson wavelet (e.g., Martelet et al., 2001; Fedi et al., 2004). The most serious error comes from using circular convolution FFT algorithms, because frequency-aliasing errors may affect the low-frequency content of the upwardly continued data at high altitudes. These errors may be kept low by performing the circular convolution on a larger area than that of interest (Oppenheim and Schafer, 1975). To this end, the input data sequences may be enlarged with known data, if available, or alternatively extended to a greater length by mathematical extrapolation by using zero-padding, maximum entropy prediction, or symmetrization. We will use this procedure throughout this paper to yield fairly accurate field continuations and DEXP estimations for synthetic or real data. For testing upward-continuation error and implications in forming a 3D data set, see Fedi and Rapolla (1999, Figures 6 and 7).

We begin with the synthetic case of a sphere, having a 1 g/cm^3 density, a 5-km radius, and its center at the position $\mathbf{r}_0(60,60,9)$ km. The gravity field was synthetically generated at 50 altitudes with a 1-km step. At each level, the data were sampled at a 1-km step along both horizontal coordinates. Figure 5 shows the field, which reaches, as expected, its maximum amplitude at $\mathbf{r}_0(60,60,0)$ km and rapidly decays either horizontally or vertically from there.

The second step scales the 3D field according to equation 10. The DEXP-transformed field is shown in Figure 6, in which the correspondence $z_0 = -z$ was used to map the DEXP-transformed field W_{g1} with respect to the z_0 axis, (i.e., along the vertical axis related to the depth to sources). The transformed field W_{g1} shows very clearly the occurrence of a high at the correct source position $\mathbf{r}_0(60,60,9)$ km. In other words, the appropriate scaling of the field versus depth is enough to disclose the depth to source of the considered potential field by a simple inspection of the extreme points of W_{g1}.

The final step computes the excess mass of the source, which amounts to 5.236×10^{14} kg. To do this, we insert the values for $W_{g1}(60,60,9) = 970.34 \times 10^{-3}$ Nm/kg and $z_0 = 9$ km in equation 20,

Table 1. One-point sources and eir scaling exponents. We describe e scaling exponents for typical classes of one-point sources. e scaling exponents are for $n = 1$, $n = 2$, $n = 3$, and for a general order n (see equations 18, 31, 34, and 36 for e classes from A to D, respectively). For comparison, Euler deconvolution S_n is also reported for n values from 1 to 3. Note at SI and scaling exponents are related by equation 35.

Source type	Source	$n = 1$ Scaling exponent	$n = 2$ Scaling exponent	$n = 3$ Scaling exponent	nth order Scaling exponent	$n = 1$ S_n	$n = 2$ S_n	$n = 3$ S_n
A	Point mass or dipole sources, spheres	1	1.5	2	$\alpha_n = 0.5(n + 1)$	2	3	4
B	Line or masses or dipoles, infinite horizontal and vertical cylinder, thin bottomless prism	0.5	1	1.5	$\alpha_n = 0.5n$	1	2	3
C	Semi-infinite plane, thin dike, sill	(0)	0.5	1	$\alpha_n = 0.5(n - 1)$, $n \geq 1$	0	1	2
D	Semi-infinite contact	(−0.5)	(0)	0.5	$\alpha_n = 0.5(n - 2)$, $n \geq 2$	−1	0	1

from which we obtain 5.237×10^{14} kg, a value very close to the correct value for the source mass excess.

As we have seen, the extreme point of W_{g1} clearly indicates the position of the source. We also observe that a spreading around the extreme point will occur, its extent depending on the depth to the source. To have some idea of this, see Figure 7 in which a dipole having a 5-km radius and a 3-A/m magnetization is considered at two different depths, i.e., first at $z_0 = 2$ km (Figure 7a and b) and then at $z_0 = 10$ km (Figure 7c and d). We see that the spreading around the maximum is limited for the shallow source, although it extends farther for the deeper location. This spreading is quite reasonable because it reflects nothing but the well-known loss of resolution of potential fields with respect to the source-measurement distance. It can, however, generate undesired interference effects in a multisource case. In the following section we describe the interference effects and examine how to circumvent the problem.

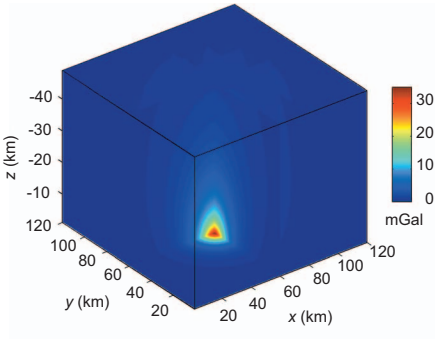

Figure 5. The gravity field due to a single pole at position $\mathbf{r}_0(60,60,9)$ km. A 3D field was synthetically generated with a 1-km step along the horizontal and vertical directions. Depths are positive and elevations are negative. The field has its maximum amplitude at the position $\mathbf{r}_0(60,60,0)$ km and rapidly decays both horizontally and vertically. As expected, the 3D field does not have clear information related to the depth to the source.

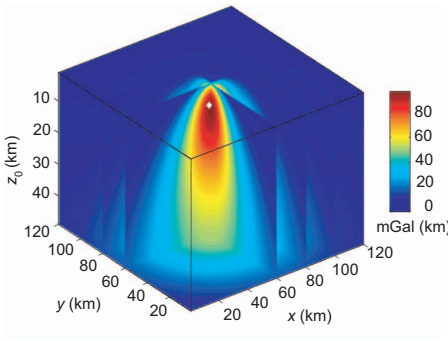

Figure 6. The scaling field W_{g1} for the model in Figure 5. Applying the DEXP transformation to the field shown in Figure 5, we obtain the scaled field W_{g1}. This field differs from the unscaled 3D field (see Figure 5) and has meaningful information related to the depth to the source. It has an extreme point (white marker) at the correct source position $\mathbf{r}_0(60,60,9)$ km. We used the correspondence $z_0 = -z$ so that the DEXP-transformed field may be mapped along the vertical axis related to the depth to sources, i.e., along axis z_0. The excess mass is fairly well-estimated from the extreme point value of W_{g1} (equation 20).

A multisource case contains sources placed at different depths with different density contrasts and masses. We consider three sources placed, respectively, at $\mathbf{r}_{01}$ (60,60,2) km, $\mathbf{r}_{02}$ (20,60,19) km, and $\mathbf{r}_{03}$ (80,60,9) km that have the following density contrasts: $\mathbf{r}_{01} = 1$ g/cm^3, $\mathbf{r}_{02} = 0.3$ g/cm^3, and $\mathbf{r}_{03} = -1.5$ g/cm^3. Their radii are $R_1 = 6$ km, $R_2 = 3$ km, and $R_3 = 3$ km, respectively. We continued the gravity field upward from zero to 50 km (Figure 8a) and performed the DEXP transformation to yield the scaled gravity field W_{g1} (Figure 8b). To perform an accurate upward continuation, the data set was enlarged with a symmetrization algorithm to a 512×512 data set. We also computed the DEXP transformation of the first-order vertical derivative of the field W_{g2} (Figure 8c) and of the second-order vertical derivative W_{g3} (Figure 8d). Our intent is to compare the DEXP transformation for different-order vertical derivatives of potential fields. For graphical simplicity, we analyze only the vertical sections of W_{g1}, W_{g2}, and W_{g3} corresponding to the profile in which $y = 60$ km (indicated with a solid red line in Figure 8a). The occurrence of three extreme points at about the right source coordinates $\mathbf{r}_{01}$, $\mathbf{r}_{02}$, and $\mathbf{r}_{03}$ is evident for W_{g1} (Figure 8b). More specifically, the highs or lows of the scaled field identify sources having, respectively, positive or negative density contrasts. We also note that W_{g1} enhances the deep-source effect with respect to the two shallower ones.

The spreading of W_{g1} around $\mathbf{r}_{01}$ is rather large but does not prevent a clear identification of the high at the right depth position of the deep source. The extent of the spreading does create a trend which somewhat affects the areas around the other two poles, $\mathbf{r}_{02}$ and $\mathbf{r}_{03}$, where interference effects arise, especially for the third source because it has a negative density contrast. The two shallow sources can be identified whether the density contrast is negative or positive. However, owing to the interference from the deep effect, the depth estimate for the third source is not as precise as that for the other two ($z_0 = 3$ km). Now, consider the DEXP transformation for the first-order vertical derivative of the field (Figure 8c). We are able to identify three extreme points also for W_{g2}, again at about the right source coordinates $\mathbf{r}_{01}$, $\mathbf{r}_{02}$, and $\mathbf{r}_{03}$. In this case, the mutual interference is considerably reduced and all the effects are better resolved. Moreover, the intensity of W_{g2} at the three extreme points is better balanced than for W_{g1}, with no evidence of one source effect dominating the others. Owing to reduced interference effects, the low associated with the deep source is now located at a more correct depth ($z_0 = 8$ km). Finally, we analyze the case of the second-order vertical

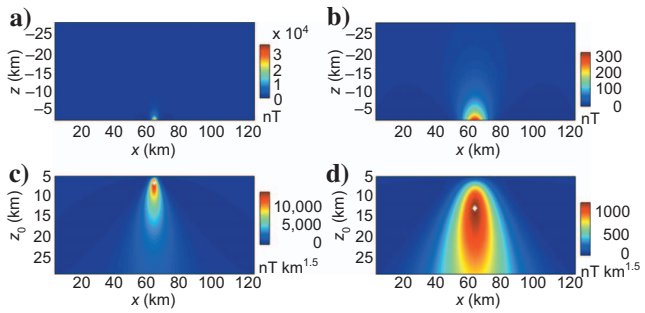

Figure 7. Spreading of scaled potential fields. We show W_{m2} for a dipole, with a 5-km radius and a 3-A/m magnetization, placed at two different depths, $z_0 = -2$ km and $z_0 = 10$ km. Although the fields (a and c) are not descriptive of the respective depths to source, W_{m2} clearly indicates the correct depths (b and d) but with a different degree of spreading around the respective extreme points.

derivative of the gravity field. Figure 8d shows the DEXP-transformed function W_{g3} in which, once again, three extreme points are evident at about the right source coordinates $\mathbf{r}_{01}$, $\mathbf{r}_{02}$, and $\mathbf{r}_{03}$. This time, however, the shallower sources are much more clearly identifiable, although the deepest one is less intense. The spreading for all three sources is quite reduced, and the mutual interference effects are practically absent. The depths estimated for any of the three sources are close to the true depths.

With regard to the estimation of excess mass values, they are quite well estimated for the three sources; the best estimations occur for the second-order derivative of the field. For the first two sources, the estimated mass excess is within 90% of the true values, whereas for the third source, we have, respectively, 10% ($n = 1$), 63% ($n = 2$), and 95% ($n = 3$) of the true value.

From this comparison, we emphasize that the high-order DEXP transformation may be useful to

1) Reduce the background and the mutual interference effects, thus allowing more accurate depth estimations
2) Obtain meaningful representations of the distribution of sources versus depth by enhancing the effects of shallow versus deep sources (the opposite occurs when using a low-order derivative)

Note that the DEXP method does not need filtering or other processes to separate, before the interpretation, the different components of the field from sources at different depths. As shown in Figure 8c and d, the results of the DEXP method enjoy an inherent stability versus high-order derivations of the field. This stability is a physical property based on the regular behavior of potential fields versus the altitude z.

For the same reasons, the DEXP method is also stable with respect to relatively high levels of noise in the data. We illustrate this in the case of a magnetic anomaly related to a homogeneous sphere (Figure 9a and b). Note that the dipolar nature of the field let two extrema to occur at the correct depth for the source, one being negative and the other positive. Adding Gaussian random noise to the data (with a 4% ratio between the respective norms), the correct position of the two extrema is, nevertheless, obtained (Figure 9b). Hence, the depth to source of dipolar anomalies is correctly estimated, even if the anomaly is not reduced to the pole. If the anomaly is not reduced to the pole, or if an asymmetric field transformation is involved, the estimate of the horizontal position of the source is not direct. The horizontal position lies, in fact, in an intermediate position with respect to the two detected extrema, which, in turn, depends on the magnetization- and inducing-field directions. For magnetic data, we can improve the location accuracy by applying the DEXP transformation to the modulus of the analytic signal of the magnetic field (Nabighian, 1972). The analytic signal of a magnetic anomaly is a bell-shaped anomaly of order $n = 3$ because it is based on the derivatives of the magnetic field. As shown in Figure 9c, DEXP transformation applied to the analytic signal still yields a good description of the source for either its horizontal or depth position, and this location is accurate even with the increase in noise associated with the derivations involved in the analytic signal transformation.

Determining the scaling exponent from the data

Here are some criteria that may be used to assess the scaling exponent directly from data.

Criterion of extreme point invariance versus derivative order

From Figure 8, we argue that changing the order of derivation n allows reduction of the mutual interference effects from nearby sourc-

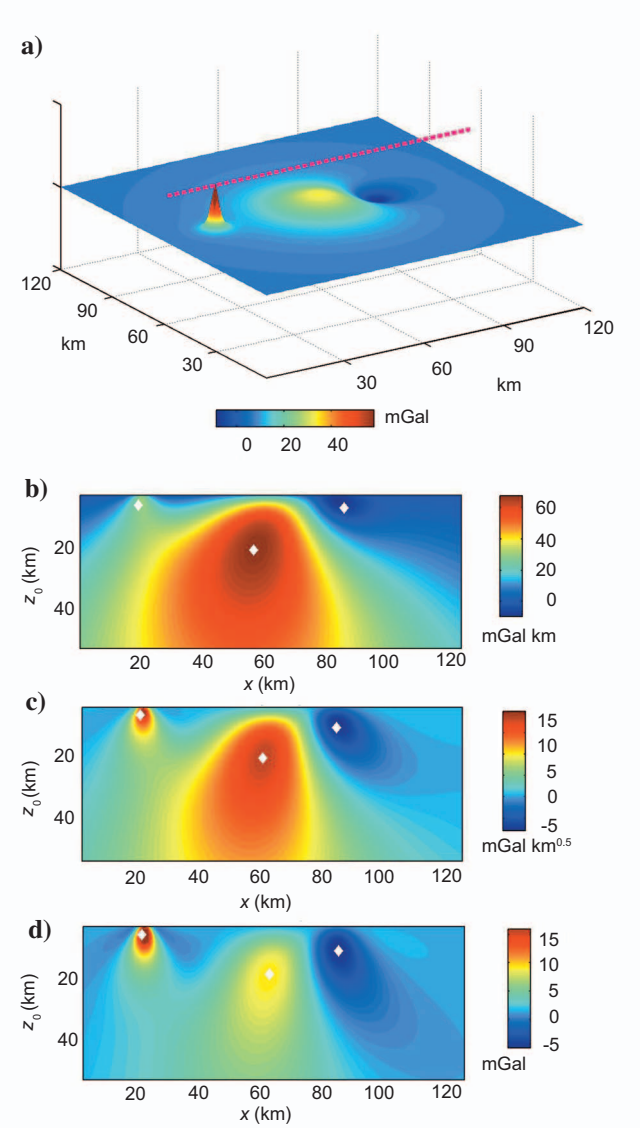

Figure 8. Scaled potential fields (gravity) of different-order n for a multisource case: (a) the field at zero-level from three pole-sources placed, respectively, at $\mathbf{r}_{01}(60,60,2)$ km, $\mathbf{r}_0(20,60,19)$ km, and $\mathbf{r}_{03}(80,60,9)$ km; and having density contrasts: $\mathbf{r}_{01} = 1$ g/cm^3, $\mathbf{r}_{02} = 0.3$ g/cm^3, and $r_{03} = -1.5$ g/cm^3; (b) scaled gravity field W_{g1}; (c) scaled vertical derivative of the gravity field W_{g2}; (d) scaled second vertical derivative of the gravity field W_{g3}. The vertical sections of W_{g1}, W_{g2}, and W_{g3} correspond to the profile shown in (a) and were obtained after numerical upward continuation of the respective fields up to 50 km and scaling by equation 18 for $n = 1$, $n = 2$, and $n = 3$, respectively. In each case, three extreme points (see white markers) indicate the presence of sources with various density contrasts, but the accuracy of the source parameter estimations (depth and mass excess) increases with the order n, especially for the third source. The figure shows that changing the order of the transformation may be useful also to reduce the mutual interference effects, to enhance the effects of shallow versus deep sources, and in general, to represent the distribution of sources versus depth without resorting to prefiltering.

es and that the position of extreme points does not change with n. We will show now that this invariance property occurs only if the correct scaling exponent is used in equation 30. This allows one to determine the scaling directly from the field data. To show this, let us consider a one-point source, e.g., a pole source and its nth-order potential field. From equation 15,

$$\tau_n = \frac{\partial \log[f_n(z)]}{\partial \log(z)} = -\frac{(n+1)z}{z - z_0}, \tag{38}$$

and $\alpha_n = 0.5(n+1)$, so that the field is

$$W_n = z^{\alpha_n} f, \tag{39}$$

whose extreme points are at

$$z = -z_0, \quad \forall\ n > 0. \tag{40}$$

But when we scale the field with different scaling exponents $\bar{\alpha}_n$, the extreme points of the scaled function $\bar{W}_n = z^{\bar{\alpha}_n} f$ will now be at

$$\bar{z}_n = -\frac{\bar{\alpha}_n z_0}{n + 1 - \bar{\alpha}_n}, \tag{41}$$

which reduces to $\bar{z}_n = -z_0$ only when $\bar{\alpha}_n = \alpha_n = (n+1)/2$.

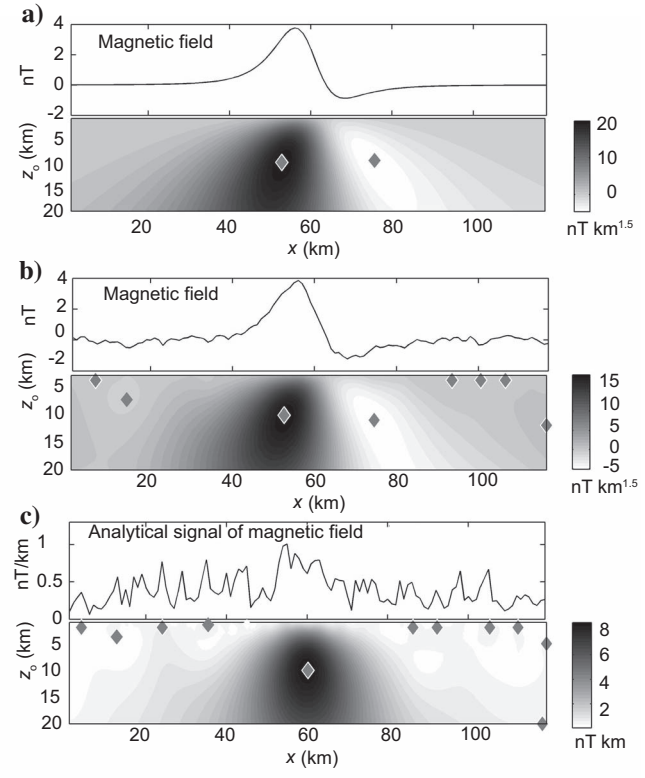

Figure 9. DEXP-transformed data for an example with a low SNR. DEXP-transformed data of the magnetic anomaly (a, top) presents two extreme points (indicated by gray markers), both at the right depth (a, bottom). Adding Gaussian white noise (b, top), the DEXP-transformed data are stable (b, bottom). Analytic signal of the anomaly has a low SNR owing to the inherent derivative computations (c, top), but the DEXP-transformed data are still stable (c, bottom), and the horizontal coordinate of the source is well-defined owing to the bell-shaped form of the analytic signal.

Hence, if we use $\bar{\alpha}_n = \alpha_n$ and consider two or more different orders n, the extreme points for the corresponding scaled potential fields will not change their position; all will be equal to the right altitude, $-z_0$. In contrast, if $\bar{\alpha}_n \neq \alpha_n$, e.g., if $\bar{\alpha}_n = 0.5n$, we see that the extreme points for the corresponding scaled potential fields will change their position according to equation 41.

Criterion of DEXP scaling-function intercept

We now derive one more criterion to determine the scaling exponent from the field data. It follows directly from the form of the scaling function. Putting $z = 1/q$, the scaling function may be rewritten from equation 38 as a function of q:

$$\tau_n(q) = -\frac{(n+1)}{1 - z_0 q}, \tag{42}$$

which means that

$$\tau_n(q \to 0) = -2\alpha_n = -S_n. \tag{43}$$

Hence, the intercept of τ_n versus q will give us an estimate of the structural index S_n; this allows the field to be scaled with $\alpha_n = 0.5S_n$. This estimate does not depend on z_0, which is unlike other theories involving the structural index, such as Euler deconvolution and CWT.

In real cases, interference from nearby sources is likely to occur, and the application of the criteria is necessarily more articulated. To show how to handle a more complex case, we describe the interpretation of magnetic data related to a basement relief feature (Figure 10), i.e., a multisource case of interest in exploration geophysics. We used the same model as Ku and Sharp (1983, their Figure 10), with the basement depth increasing from 6000 ft (1.83 km) to 12,000 ft (3.65 km) below the measurement surface. The basement interface represents normal faults inclined at various angles with respect to a horizontal ground surface at 1.83 km. with a 10^{-3} cgs susceptibility

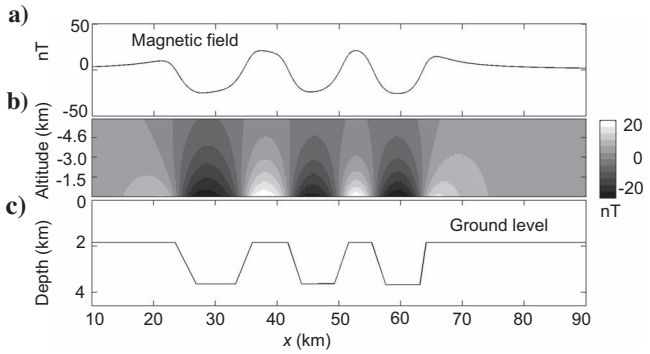

Figure 10. The magnetic anomaly from a faulted basement. The magnetic anomaly (a) is shown as a result of the faulted basement interface shown in (c). The field is measured 1.83 km above the ground. Susceptibility contrast is 0.0126 SI. Inducing magnetic field intensity is 50,000 nT with a 5° declination and a 45° inclination. Profile azimuth is 90°. The anomaly presents a series of highs and lows related to those of the basement. Also shown is (b) the field continued by 2D numerical upward continuation up to 6.1 km with a 0.15-km step.

contrast (0.0126 SI). Application of Werner Deconvolution (Ku and Sharp, 1983) yielded solutions grouped toward the top edge of the interface because the horizontal separation between the top and bottom edges was judged by the authors to be not large enough to give the necessary resolution.

In contrast, the DEXP method provides meaningful results. The two ends of the source are the less disturbed parts of the profile. Hence, they may be analyzed by using the derivative criterion. In fact, changing the order n from two (magnetic field) to four and using the scaling exponent for class C [$\alpha_n = 0.5(n - 1)$], we obtain rather stable positions of the extreme points of the DEXP-transformed scaled field (Figure 11), with x_0 ranging from 65 to 68 km and z_0 from 1.60 to 2.2 km. Better estimates will be obtained using the second criterion. The rest of the profile corresponds to a higher degree of mutual interference from the deeper and the shallower basement, with the degree of interference decreasing as n increases. Because of this, it is convenient to use the second criterion at different orders of n. At $n = 2$ (magnetic field) we obtain a meaningful result. The field appears as a sequence of highs and lows (Figure 12a), and the second criterion yields (Figure 12b) a structural index of about two for all such lows and highs, corresponding to class B ($S_2 = 2$, $\alpha_2 = 1$; see Table 1). The scaling function τ_2 was computed using vertical profiles above each low and high. The DEXP results (Figure 12c) depict quite closely the whole structure of the basement because extreme points occur close to the upper and lower parts of the basement. This is an important result because it describes not only the shallowest features, as did the Werner deconvolution (Ku and Sharp, 1983), but also the deeper ones. At highest orders (e.g., $n = 8$), we may expect that the degree of interference is so reduced that the derived fields will mainly show the effects of the shallowest parts of the basement (Figure 12d). Using again the second criterion (Figure 12e), we find for all the upper corners a 6.5 intercept, which indicates a structural index: $n - 2 + 0.5$, which is between classes C and D (Table 1). It is slightly lower than that (corresponding to class C) previously estimated with the first criterion for the external corner. Scaling the derived field with this value, we find fairly good depth estimates for the upper corners (Figure 12f). The accurate numerical computation of the sixth-order vertical derivative of the magnetic field (shown in Figure 12d) was obtained using the ISVD algorithm (Fedi and Florio, 2001) and a piecewise polynomial form of cubic smoothing splines.

In conclusion, using both the criteria, we may satisfactorily reconstruct the kind and the geometry of the basement, as shown in Figure 13, in which we compare the extreme points from the previous analyses versus the actual basement depth. This example shows that the DEXP method is able to resolve variable basement depths.

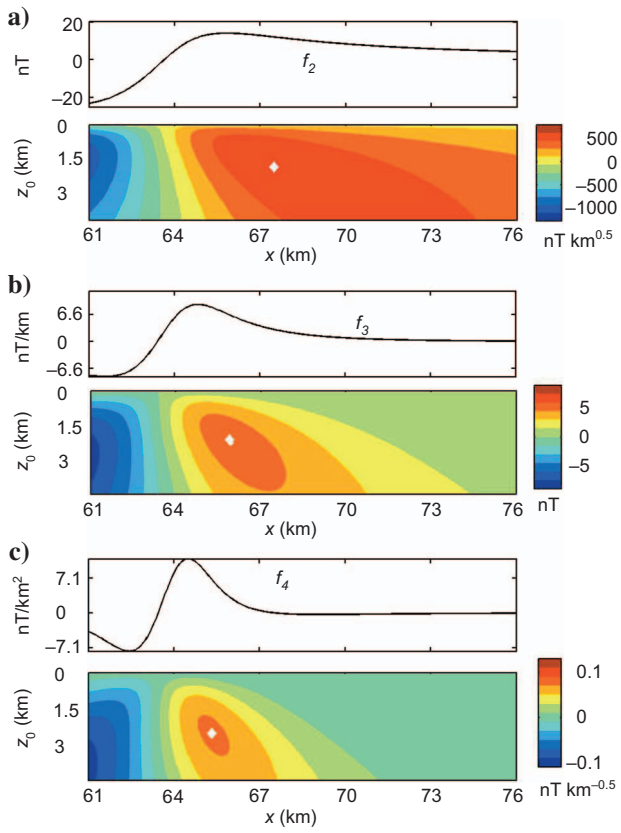

Figure 11. Application of the DEXP extreme-point invariance to a buried magnetic dipole. The magnetic field and its first- and second-vertical derivatives are shown at the tops of (a), (b), and (c), respectively. The order of the field n varies from 2 to 4 accordingly. Their DEXP-transformed data are at the bottom, computed from the upward-continued field shown in Figure 10b (61 km $< x <$ 76 km) and with the scaling law of class C [$\alpha_n = 0.5(n - 1)$, see Table 1]. Extreme point positions are rather stable, so they yield an approximate depth estimate. We can have more refined estimates if we apply the criterion of scaling to the function intercept (see Figure 12f).

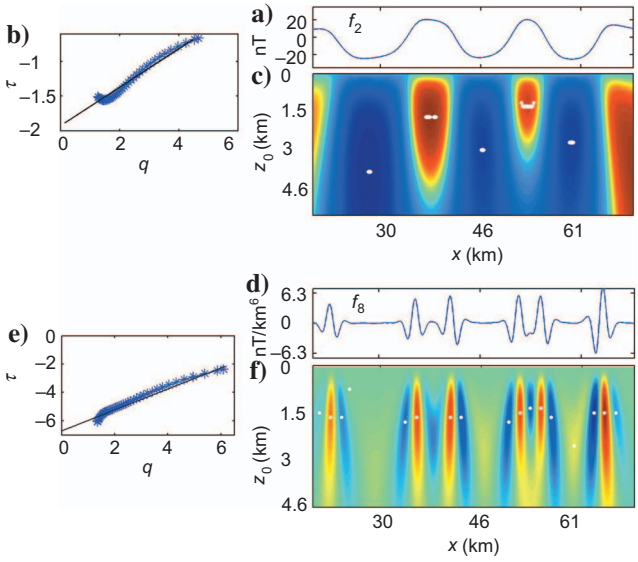

Figure 12. Application of the DEXP scaling-function intercept. The criterion is applied to the numerically upward-continued field shown in Figure 10b and to its sixth-order derivative corresponding to $n = 2$ and $n = 8$, respectively. Zero-level profiles are shown in (a) and (d) for $n = 2$ and $n = 8$, respectively. From equation 43, we know that the scaling exponent may be estimated as one-half of the intercept of $\tau_n(q)$ versus q, as shown in (b) and (e), respectively. From Table 1, we obtain class B ($S_2 = 2$, $\alpha_2 = 1$) for the magnetic field and an intermediate value between classes C and D ($S_8 = 6.5$, $\alpha_8 = 3.25$) for the sixth-order vertical derivative of the magnetic field. (c) The DEXP-transformed data of order $n = 2$ depicts quite closely the whole structure of the basement because extreme points occur close to the upper and lower parts of the basement. (f) The DEXP-transformed data of order $n = 8$ yields rather accurate depth estimates for the upper corners of the basement.

APPLICATION TO REAL CASES

We apply now the method to the real case of the Campanian Plain Bouguer gravity data (southern Italy). The gravity field shown in Figure 14 is a residual field after subtraction of a long-wavelength trend (Rapolla et al., 1989).

The Campanian Plain is a Plio-Pleistocene, northwest-southeast-stretched, tectonic depression that is bounded to the northwest, northeast, and southeast by Mesozoic carbonate platforms and to the southwest, by the Tyrrhenian Sea. Some authors have reported a maximum depth of the carbonate platforms in this area of about 5 km (Ippolito et al., 1973). Overlying the carbonates are sediments of alluvial and volcanic origin. Within the Campanian Plain, there are Quaternary volcanic areas, including the Somma-Vesuvius and the Phlegrean volcanic district.

The plain is characterized by a broad Bouguer anomaly low, which includes the area of the town of Naples, between Phlegrean Fields and Somma-Vesuvius (Figure 14). Rapolla et al. (1989) separated the various gravity effects from shallow, intermediate, and deep sources by means of Fourier band-pass filtering of the Bouguer gravity data. At high frequencies, a complex pattern of highs and lows accounts for the shallow distribution of sedimentary basins, grabens, and either volcanic or carbonate rocks. A broad low centered in the Neapolitan area characterized instead the field at mid- to longer wavelength (Rapolla et al., 1989, their Figure 4), which they related to a large amount of low-density, molten trachybasalts, with a -0.2 g/cm^3 density contrast, at 12-km depth. This source was hypothesized by Rapolla et al. (1989) as a possible magmatic reservoir feeding the eruptive centers of the whole Campanian volcanic region.

We applied the DEXP transformation to the gravity field of the Campanian region without resorting to prefiltering. We analyzed the scaled potential fields at several orders and show the results for $n = 3$ (Figure 15). In agreement with the criteria established in the previous section, a scaling exponent of class B ($\alpha_1 = 1.5$; see Table 1) seemed appropriate for most of the sources. The positions of such sources are obtained from the extreme point locations of W_{g3} (Figure 15, extrema are marked by white symbols) along the two cross sections indicated in Figure 14. A complex pattern of either deep or shallow sources appears; this confirms the ability of the method to describe the effects at any depth without prefiltering. This is a strength of the DEXP transformation; it implies that the method may be applied to a multisource case without the need to separate the different-depth-source effects through methods such as polynomial, Fourier, or wavelet analysis. The main features are shallow lows corresponding to several basins, such as Acerra and Pompeii, and a relatively deep low (at about $x = 70$ km, $y = 100$ km, and $z_0 = 12$ km) corresponding to the deep source already identified in the previous studies. Among the extreme points of shallow sources, notice those related to Mt. Massico (northeast of Naples) and to the Sorrento Peninsula (northwest of Naples) carbonates, which are located at both the ends of the section.

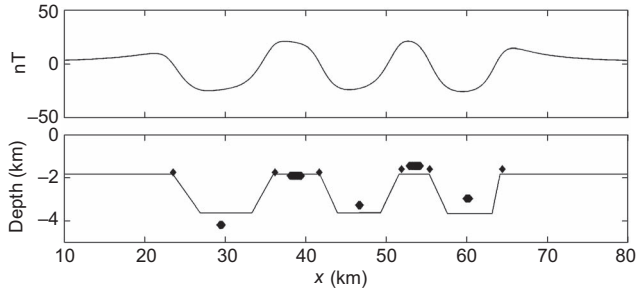

Figure 13. DEXP reconstruction of the magnetic basement. Using the depth estimates (black diamonds) from the DEXP data shown in the previous figures, a fairly good reconstruction of both the shallow and deep features of the magnetic basement (solid line) is obtained.

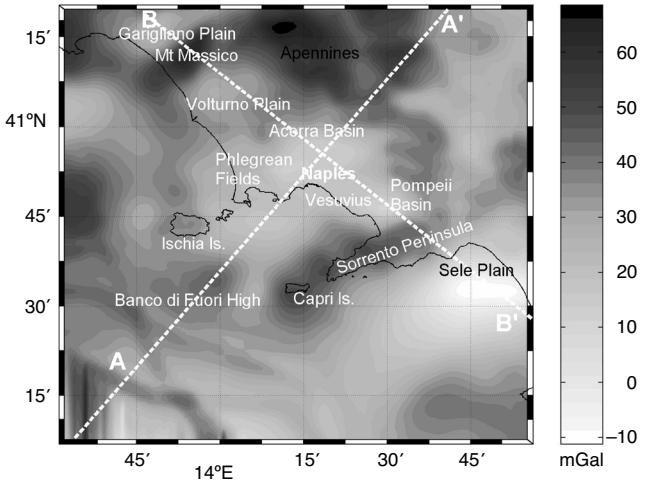

Figure 14. The Bouguer gravity field of the Campanian area (southern Italy). The map is characterized by a rather complex pattern of lows, such as those of Pompeii and Acerra, and highs mostly related to carbonate rocks exposed at the surface, such as the first Apennines reliefs, the Sorrento Peninsula, and Mt. Massico.

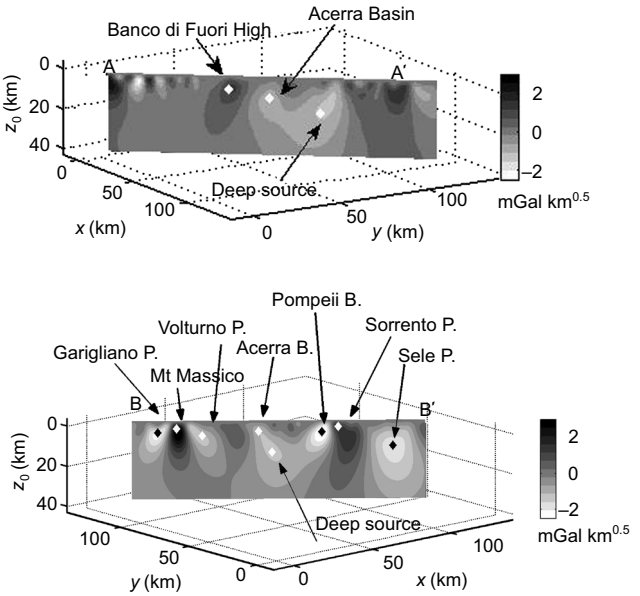

Figure 15. Sections of W_{g3} for the Bouguer anomaly field profiles of Figure 14. Deep and shallow sources may be observed; they have either a positive or negative density contrast. White markers indicate DEXP extreme points. Shallow lows correspond to Acerra, Pompeii, and other basins, whereas a relatively deep, extreme-point low (at about $x = 70$ km, $y = 100$ km, and $z_0 = 12$ km) marks the deep source described in the text. Shallow extreme-point highs also occur, mainly indicating Mesozoic carbonate platforms, such as Mt. Massico (northeast of Naples) and the Sorrento Peninsula (northwest of Naples). Note section locations in Figure 14.

CONCLUSIONS

We have described the theory and the applications of DEXP transformation that allows us to estimate depth to the sources of potential field anomalies, the excess of the mass (gravity case) or the dipole moment intensity (magnetic case), and the kind of source. The transformation involves scaling the field by power laws of the altitudes, the scaling exponent being dependent on the order n of the vertical derivative of the potential field and on the source type (or source class, see Table 1). Criteria are given to determine the correct scaling exponent from real data and, thereby, to identify the kind of source. The criteria are respectively based on the invariance of the estimated depth to source with respect to the order of the DEXP transformation and on the evaluation of the scaling exponent intercept.

A meaningful relationship was shown between scaling exponents α_n and S_n (the structural index of the Euler deconvolution), which is based on the fact that both S_n and α_n are source parameters reflecting the type of source and the falloff rate of their fields. This relationship may be extended to a further source parameter, namely the scaling exponent β involved in the theory of the CWT (using the Poissonian wavelets), which is associated with the degree of homogeneity of the source and with the structural index itself.

We note some other remarkable features of the DEXP transformation: First, it is inherently stable with respect to the noise level and to the derivation order of the field. This stability, not completely shared by Euler deconvolution or other methods, is based on the regular behavior of potential fields versus the altitude z. Owing to this stability, we may apply the DEXP transformation to rather high-order-derived potential fields, thus allowing improved resolution and estimates of source parameters for the multisource case. An additional property is that the scaled field yields a significant description of the depth positions of the different sources, no matter if a separation filter has been used in advance. Finally, we note that the DEXP transformation is simple to implement and very fast. Interpretation based on the DEXP transformation may be, therefore, considered as a suitable first step for interpreting potential field anomalies before using more refined modeling procedures.

ACKNOWLEDGMENTS

I thank the associate editor John W. Peirce and the anonymous reviewers for their suggestions and especially for having stimulated me to develop the part of this paper related to determining the structural index from the data.

REFERENCES

Baranov, W., 1975, Potential fields and their transformations in applied geophysics: Gebruder-Borntraeger.
Cooper, G. R. J., 2004, Euler deconvolution applied to potential field gradients: Exploration Geophysics, **35**, 165–170.
Fedi, M., and G. Florio, 2001, Potential fields source boundaries detection by an enhanced horizontal derivative: Geophysical Prospecting, **49**, 13–25.
Fedi, M., R. Primiceri, T. Quarta, and A. V. Villani, 2004, Joint application of continuous and discrete wavelet transform on gravity data to identify shallow and deep sources: Geophysical Journal International, **156**, 7–21.
Fedi, M., and A. Rapolla, 1999, 3-D inversion of gravity and magnetic data wi dep resolution: Geophysics, **64**, 452–460.
Hornby, P., F. Boschetti, and F. G. Horovitz, 1999, Analysis of potential field data in e wavelet domain: Geophysical Journal International, **137**, 175–196.
Ippolito, F., F. Ortolani, and M. Russo, 1973, Struttura marginale del' Appennino Campano: Reinterpretazione dei dati di antiche ricerche di idrocarburi: Memorie Società Geologica Italiana, **XII**, 227–250.
Keating, P., and M. Pilkington, 2004, Euler deconvolution of e analytic signal and its application to magnetic interpretation: Geophysical Prospecting, **52**, 165–182.
Kellogg, O. D., 1967. Foundations of potential eory: Springer Publishing Company, Inc.
Ku, C. C., and J. A. Sharp, 1983, Werner deconvolution for automated magnetic interpretation and its refinement using Marquardt's inverse modeling: Geophysics, **48**, 754–774.
Martelet, G., P. Sailhac, F. Moreau, and M. Diament, 2001, Characterization of geological boundaries using 1-D wavelet transform on gravity data: eory and application to e Himalayas: Geophysics, **66**, 1116–1129.
Mushayandebvu, M. F., P. van Driel, A. B. Reid, and J. D. Fairhead, 2001, Magnetic source parameters of two-dimensional structures using extended Euler deconvolution: Geophysics, **66**, 814–823.
Nabighian, M. N., 1972, e analytic signal of two-dimensional magnetic bodies wi polygonal cross-section: Its properties and use for automated anomaly interpretation: Geophysics, **37**, 507–517.
Oppenheim, A. V., and R. W. Schafer, 1975, Digital signal processing: Prentice Hall.
Parker, R. L., 1977, Understanding inverse eory: Annual Review of Ear and Planetary Sciences, **5**, 35–64.
Rapolla, A., M. Fedi, and G. Fiume, 1989, Crustal structure of e Ischia-Phlegrean fields geoermal area, near Naples (Italy), from gravity and aeromagnetic data: Geophysical Journal, **97**, 409–419.
Reid, A. B., J. M. Allsop, H. Granser, A. J. Millett, and I. W. Somerton, 1990, Magnetic interpretation in ree dimensions using Euler deconvolution: Geophysics, **55**, 80–91.
Sailhac, P., and D. Gibert, 2003, Identification of sources of potential fields wi e continuous wavelet transform: Two-dimensional wavelets and multipolar approximations: Journal of Geophysical Research, **108**, B5 2262.
Salem, A., and D. Ravat, 2003, A combined analytic signal and Euler meod (AN-EUL) for automatic interpretation of magnetic data: Geophysics, **68**, 1952–1961.
Stavrev, P. Y., 1997, Euler deconvolution using differential similarity transformations of gravity or magnetic anomalies: Geophysical Prospecting, **45**, 207–246.
Telford, W. M., L. P. Geldart, and R. E. Sheriff, 1990, Applied geophysics: Cambridge University Press.